Biosensors and Bioelectronics 267 (2025) 116807

Contents lists available at ScienceDirect

Biosensors and Bioelectronics

journal homepage: www.elsevier.com/locate/bios

Bridging basic science and applied diagnostics: Comprehensive viral diagnostics enabled by graphene-based electronic biosensor technology advancements

Anna Nele Herdina [a,1], Anil Bozdogan [a,b,1], Patrik Aspermair [b,c], Jakub Dostalek [c,d], Miriam Klausberger [e], Nico Lingg [f,g], Monika Cserjan-Puschmann [f,g], Patricia Pereira Aguilar [f,g], Simone Auer [b], Halil Demirtas [b], Jakob Andersson [b,h], Felix Lötsch [i,j], Barbara Holzer [k], Adi Steinrigl [l], Florian Thalhammer [m], Julia Schellnegger [a], Monika Breuer [a], Wolfgang Knoll [b,c], Robert Strassl [a,*]

[a] Department of Laboratory Medicine, Division of Clinical Virology, Medical University of Vienna, Vienna, Austria
[b] BioSensor Technologies, Austrian Institute of Technology, Vienna, Austria
[c] Life Sciences Technology, Danube Privat University, Wiener Neustadt, Austria
[d] Institute of Physics, Czech Academy of Sciences, Prague, Czech Republic
[e] Department of Biotechnology, BOKU University, Vienna, Austria
[f] ACIB - Austrian Centre of Industrial Biotechnology, Vienna, Austria
[g] Department of Biotechnology, Institute of Bioprocess Science and Engineering, BOKU University, Vienna, Austria
[h] Institute of Science and Technology Austria, Klosterneuburg, Austria
[i] Division of Clinical Microbiology, Medical University of Vienna, Vienna, Austria
[j] Division of Infectious Diseases and Tropical Medicine, Medical University of Vienna, Vienna, Austria
[k] Institute Krems Bioanalytics, IMC Krems University of Applied Sciences, Krems, Austria
[l] Austrian Agency for Health and Food Safety (AGES), Institute for Veterinary Disease Control Mödling, Mödling, Austria
[m] Department of Urology, Medical University of Vienna, Vienna, Austria

ARTICLE INFO

Keywords:
Graphene field-effect transistor
COVID-19
SARS-CoV-2
Infectivity
Diagnostics
Nucleocapsid protein

ABSTRACT

This study presents a graphene field-effect transistor (gFET) biosensor with dual detection capabilities for SARS-CoV-2: one RNA detection assay to confirm viral positivity and the other for nucleocapsid (N-)protein detection as a proxy for infectiousness of the patient. This technology can be rapidly adapted to emerging infectious diseases, making an essential tool to contain future pandemics. To detect viral RNA, the highly conserved E-gene of the virus was targeted, allowing for the determination of SARS-CoV-2 presence or absence using nasopharyngeal swab samples. For N-protein detection, specific antibodies were used. Tested on 213 clinical nasopharyngeal samples, the gFET biosensor showed good correlation with RT-PCR cycle threshold values, proving its high sensitivity in detecting SARS-CoV-2 RNA. Specificity was confirmed using 21 pre-pandemic samples positive for other respiratory viruses. The gFET biosensor had a limit of detection (LOD) for N-protein of 0.9 pM, establishing a foundation for the development of a sensitive tool for monitoring active viral infection. Results of gFET based N-protein detection corresponded to the results of virus culture in all 16 available clinical samples and thus it also proved its capability to serve as a proxy for infectivity. Overall, these findings support the potential of the gFET biosensor as a point-of-care device for rapid diagnosis of SARS-CoV-2 infection and indirect assessment of infectiousness in patients, providing additional information for clinical and public health decision-making.

* Corresponding author. Medical University of Vienna, Division of Clinical Virology – 4P, Waehringer Guertel 18-20, 1090, Vienna, Austria.
E-mail address: Robert.strassl@meduniwien.ac.at (R. Strassl).
[1] These authors contributed equally to this work.

https://doi.org/10.1016/j.bios.2024.116807
Received 9 July 2024; Received in revised form 2 September 2024; Accepted 19 September 2024
Available online 21 September 2024

1. Introduction

The coronavirus disease 2019 (COVID-19) pandemic has accelerated advancements in technologies for detecting severe acute respiratory syndrome coronavirus 2 (SARS-CoV-2) (Rabiee, 2020; Soler, 2020; Mathuria et al., 2020; Karkan et al., 2022). The World Health Organization (WHO) and health agencies prioritize nucleic acid amplification tests (NAAT) like real-time polymerase chain reaction (RT-PCR) as the gold standard for detecting SARS-CoV-2 due to their high sensitivity and specificity (World Health Organisation WHO, 2021). However, while RT-PCR can detect viral RNA, it does not necessarily confirm the presence of replicative virus, complicating the assessment of infectiousness and risk of transmission. Virus propagation in culture is the preferred method to test for replicative virus (Lu et al., 2020; Gaspar et al., 2001; Compans and Choppin, 1967), but it is labor-intensive and time-consuming and therefore not suitable for routine diagnostics. Furthermore, it is necessary to propagate infectious virus in a biosafety level three (BSL3) containment usually restricted to specialized institutions. Consequently, semi-quantitative RT-PCR thresholds based on virus culture and RT-PCR cycle threshold (Ct) values were implemented as proxy for infectivity but these must be interpreted carefully within the history of infection, the non-standardizable nature of respiratory samples and variability of different RT-PCR assays on the market (Arnaout et al., 2021; Kirby et al., 2023). Moreover, persistent or intermittent positive RT-PCR results pose particular challenges in clinical settings, potentially leading to prolonged isolation and strained hospital resources (Mencacci et al., 2021; Avanzato et al., 2020).

This highlights the need for a comprehensive approach with the potential to answer the question whether the sample contains replicative virus and thus indicating the risk of transmission. We focused on the nucleocapsid (N-) protein, highly conserved across SARS-CoV-2 variants and abundant in the virus (Muradyan et al., 2024), because the presence of non-denatured viral protein/RNA complex is established as a potentially reliable marker for intact infectious virus as opposed to residual viral RNA (Wu et al., 2023; Diao et al., 2021).

Biosensor technologies have been pursued for virus detection, utilizing biomarker-specific recognition elements, transducers, and sensor read-out systems. Examples include P-FAB for saliva testing, eCovSens for spike protein detection in saliva, and surface plasmon resonance (SPR) spectroscopy biosensors for detecting SARS-CoV-2 antibodies in serum (Murugan et al., 2020; Zhen et al., 2020; Seo, 2020; Mahari, 2020); these sensors utilizing nanomaterials have shown promise for precise viral detection (Djaileb et al., 2020; Qiu, 2020; Roether, 2019; Rampazzi, 2016). However, integrating biosensors into diagnostic procedures faces challenges like device inconsistencies and sample complexity.

To address these issues, we developed a device using graphene field-effect transistor (gFET) biosensor technology with dual target detection for SARS-CoV-2 diagnosis. We chose gFET technology over other sensor types due to graphene's unique electronic properties and ease of functionalization (supplemental information [SI] 2.5). Our device includes two gFET assays for nasopharyngeal swab specimens: one for detecting SARS-CoV-2 RNA by targeting a conserved region in the SARS-CoV-2 genome (E-gene) (Corman et al., 2020) and monitoring shifts in the Dirac point voltage, and another for detecting the nucleocapsid protein (N-protein) (Kirby et al., 2023) indicative of infectivity by monitoring changes in current from transfer characteristics (I_dV_g). We improved gFET biosensor accuracy and reliability by using NaCl calibration (see SI 2.3) to standardize responses and reduce device-to-device variability. Additionally, a differential biosensing strategy, involving baseline establishment with pooled negative samples and subsequent target detection, effectively mitigated non-specific binding and environmental noise, ensuring robust SARS-CoV-2 detection even in complex biological matrices.

2. Material and methods

2.1. Clinical patient samples

We used 242 archived nasopharyngeal swab samples (NaCl or Copan UTM) from routine RT-PCR testing between Oct 2020–May 2023 at the Division of Clinical Virology. For SARS-CoV-2 E-gene RNA detection, 213 heat-inactivated samples were tested (heat inactivation see SI 1.1 (Loveday et al., 2021; Batéjat et al., 2021)), including 32 RT-PCR positive samples covering the linear range (Ct 12.1 to 39.0) of the SARS-CoV-2 RT-PCR (various variants, see detailed in SI section 1) and 160 RT-PCR negative samples pooled in groups of five. Specificity testing of the SARS-CoV-2 E-gene assay on the gFET biosensor device was carried out using 21 pre-pandemic samples (pooled), that tested RT-PCR positive for respiratory viruses other than SARS-CoV-2 (influenza A, influenza B, respiratory syncytial virus, rhinovirus, metapneumovirus, adenovirus or enterovirus; see SI section 1.1). N-protein detection for infectivity was conducted on 29 non-heat-inactivated samples from 18 patients (28 positive, 1 negative, Table 1), with a focus on Ct values > 30. Virus culture results were available for 16 samples (12 patients; SI 1.5).

2.2. gFET biosensor

Signal transduction was based on the MOSFET equation. Calibration was performed using NaCl solutions of known concentrations (SI 2.3, Suppl. Fig. 3) before functionalizing the graphene surface with synthetic DNA or anti-N protein antibodies. We used 0.01x PBS buffer and polyethylene glycol (PEG) to address Debye screening and prevent nonspecific binding (for Debye length calculation see SI 2.4). A differential biosensing methodology was adopted, involving sequential exposure to negative and positive samples to enhance specificity (SI 2.6).

$$I_{DS} = \mu\, C_{ox}\, \frac{W}{L}\, (V_G - V_T)\; V_{DS}$$

In this equation, W (m) represents the channel width, L (m) stands for the channel length, C_{ox} (F/cm^2) is the capacitance of the insulating layer, μ (cm^2/V.s) refers to the charge mobility of the semiconductor, V_T (V)is the threshold voltage, V_G (V) denotes the gate voltage, and V_{DS} (V) signifies the drain-source voltage. Any surface event occurring at the gate-electrolyte interface is linked to a change in C_{ox}, which in turn results in an alteration of I_{DS} (A).

To monitor the bio-interaction, the transfer characteristic of the gFET (I_dV_g) was recorded with a Keysight U2722A modular source/measure unit (Keysight Technologies, USA) and a LabView-based software (National Instruments, USA) developed by our group. The schematic transistor architectures for bio-sensing are shown in Fig. 1a. They consist of a graphene channel between the drain and source electrode, a liquid gate electrode silver wire, coated with silverchloride (SI 2.5, Suppl. Figs. 4 and 5). The gate electrode is exposed to the liquid ion channel, therefore to the analyte (Fig. 1a). A specific range of gate voltages (−800 mV to +800 mV) at a scan rate of 20 mV/s with V_{DS} = 50 mV was used as system parameters (Reiner-Rozman et al., 2021; Kissmann et al., 2022; Rodrigues et al., 2021; Hasler, 2022). I_dV_g were recorded and averaged for each step. Stability analysis of the gFET was performed by recording a set of I_dV_g every 20 min in running buffer for 3 h (SI 2.6 & 2.7, Suppl. Figs. 5 and 7). A time-resolved measurement method was not used in this study because a fixed gate voltage during measurements was necessary to ensure consistent results. Applying a gate voltage during functionalization or exposition of the surface to samples, however, could potentially interfere with the immobilization process by altering the electrostatic interactions between the graphene surface and the charged biomolecules.

To functionalize the surface of rGO, a non-covalent approach was used with 1-pyrenebutyric acid (PBA) and Pyrene-PEG-alcohol (PyPEG)

Table 1
Nucleocapsid-protein detection for infectivity determination - in context with viral cell culture, RT-PCR, patient medical history, and sampling timepoints.

Patient no	SARS-CoV-2 variant	Sex	Age	Vaccinations	Comorbidities/risk factors	Initial symptoms	Peak viral load PCR Ct	Symptoms	Days before/after peak viral load	Sampling day after diagnosis	PCR Ct	Cell culture	gFET
Patients with virus culture tested samples													
1	WT	f	88	0	Cor, DM	0	15.04	0	−3	d0	31.96	–	negative
								9	0	d3	15.04	positive	positive
								8,9,11	10	d13	25.43	negative	negative
2	Alpha	f	56	0	Ca	2,6	18.99	1,2,8	0	d4	18.99	positive	positive
								0	10	d14	30.83	negative	negative
3	Alpha	m	71	0	Ad, Cor, Vasc	1,2,7	17.83	1,2,6,7	0	d2	18.73	positive	positive
								1,2,7,8,9	9	d11	27.66	negative	negative
4	WT	m	51	0	Cor, DM, Ren, Hema	1,2,4,7	19.21	1,2,4,9	−2	d2	29.9/ 33.6	–	negative
								2,9,11	3	d7	21.12	positive	positive
								9	11	d15	34.42	negative	negative
7	Alpha	f	82	0	Cor	1,5,6,8,9	15.18	1,6,8,9	2	d4	16.7	positive	positive
8	WT	m	66	0	SOT (kidney), Vasc	11	15.24	2,7,9,11	26	d4	19.45	positive	positive
9	Alpha	m	80	0	Cor, Hema, Vasc, Pulm	1,3,4,6,7	16.87	0	15	d17	neg.	negative	negative
10	WT	m	89	0	Cor, Vasc, Uro	1,4,6,7	28.64[a]	1	unknown[a]	d79	32.82	negative	negative
11	Alpha	m	52	0	Ad, DM, Ca	1,4,9,11	16.20	1	19	d20	35.07	negative	negative
12	Alpha	m	22	0	none	1,2,4,6,7,9	22.01	9	7	d15	33.38	negative	negative
13	Alpha	f	81	2	Cor, Hema, Vasc, GI	1,9,11	14.57	1	15	d15	31.92	negative	negative
14	Alpha	f	71	0	none	1,2,4,6,7,9,11	23.87	1,2,6,7,9	10	d20	33.88	negative	negative
Patients without virus culture tested samples													
5	WT	f	60	0	DM, COPD, Hema	8,9,10,11	18.28	8,10,11	−1	d4	34	–	positive
								6,8,10,11	0	d5	18.28	–	positive
								6,8,10,11	1	d6	19.05	–	positive
								6,8,10,11	9	d14	34.63	–	negative
								8,10,11	11	d16	39.3	–	negative
6	WT	m	85	0	DM, Ren, Neur, GI	5,9	15.33	5,9	0	d7	15.33	–	positive
								1	12	d19	33.98	–	negative
15	WT	f	47	0	Cor, Uro, Ca, Ren, Neur, Gyn, Pulm	1,7	15.99	1,7	−8	d1	27.7	–	positive
16	Omicron (BA.4/5)	m	86	3	Ad, Ren, Vasc, septic HTEP	2	18.45	2	−2	d0	39.5	–	positive
17	Omicron (BA.2)	f	78	4	Ca, Hema, GI	6,8,9,11[b]	unknown[b]	6,9,11	unknown[b]	d34	23.45	–	positive
18	Omicron (XBB 1.5)	f	52	unkn[x]	Cor, SOT (heart), Ren	1,2,4,6,9	12.21	1,2	15	d16	16.2	–	negative

Abbreviations: Clinical symptoms and treatments: O2 given 1, pneumonia (X-ray) 2, emphysema (X-ray) 3, fever 4, subfebrile 5, cough 6, dyspnea 7, pain 8, fatigue 9, anosmia/ageusia 10, gastrointestinal symptoms 11, asymptomatic 0.
Comorbidities and risk factors: adipositas Ad, cancer Ca, coronary Cor, Diabetes mellitus type II DM, gastrointestinal GI, gynecological Gyn, total hip endoprosthesis HTEP, hematological Hema, neurological Neur, renal Ren, solid organ transplant SOT, pulmonary Pulm, urological Uro, vascular Vasc.
[x] Patient 18: Vaccination status of patient not disclosed in medical histor
[a] Patient 10: Ct value on day 2 of hospital admission; initial SARS-CoV-2 diagnosis 66 days before hospital admission (no information before and on previous PCR Ct values as patient was treated elsewhere).
[b] Patient 17: Initial symptoms from day of hospital admission from home with (Post-)COVID-19, day 33 (symptoms persistent since diagnosis according to patient; no information on previous PCR Cts, as patient was treated elsewhere), patient transferred to other hospital on day 37.

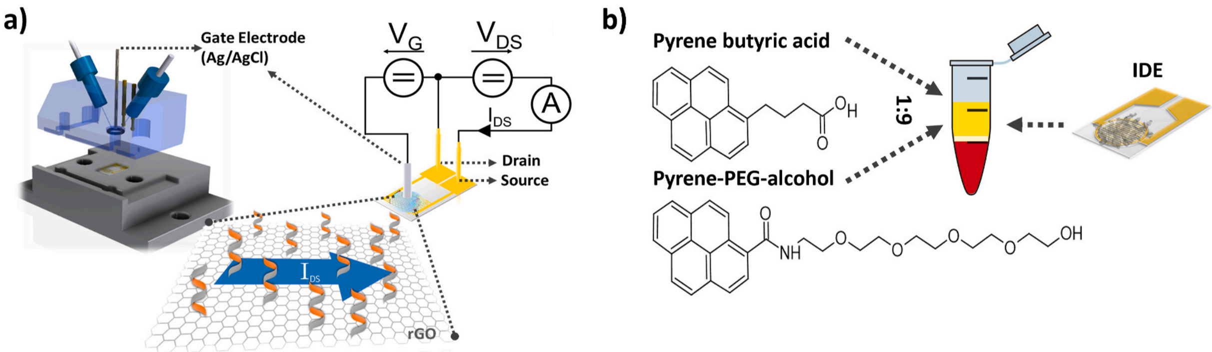

Fig. 1. Schematic representation of the used surface structure with functional groups a) gFET based biosensor measurement system, custom produced flowcell by Micrux; interdigitated electrodes with a 5 μm gap between the electrodes, coated with a reduced graphene oxide (rGO). b) functionalization utilizing π-π stacking on the rGO layer with Pyrene butyric acid and Pyrene-PEG-alcohol (chemical structures were drawn with ACD/ChemSketch).

which relies on π-π stacking (Fig. 1b; for description of electrode surface preparation and graphene oxide deposition and reduction see SI 2.1&2.2 and Suppl. Figs. 1 and 2). The PBA and PyPEG mixture was prepared at 1 mM at a 1:9 ratio respectively in anhydrous DMSO and then applied to rGO-coated chips overnight. The chips were thoroughly rinsed with EtOH before activation. The first step in biofunctionalizing graphene on the gFET is to modify it with pyrene-carboxylic acid. The linker, PBA, forms a non-covalent bond (π-π stacking) with the pyrene anchor to rGO. The carboxylic-acid (-COOH) can then form an amide bond to biorecognition elements after an activation step with 1-ethyl-3-(3-dimethylaminopropyl)carbodiimide/*N*-hydroxysuccinimide (EDC/NHS, see Fig. 2a and Suppl. Fig. 6) and PyPEG contains hydroxyl (-OH) groups that remain non-reactive but provide an antifouling effect by creating a hydrophilic barrier. These changes enable the gFET to detect bioreceptor-analyte binding events, due to two main effects: graphene doping, which involves direct charge transfer between the bioreceptor-analyte complex and the graphene channel, and electrostatic gating, which involves the accumulation of charges on the graphene surface upon binding.

3. Results

3.1. Semi-quantitative nucleic acid detection - SARS-CoV-2 E-gene RNA

To activate -COOH groups, chips were incubated for 15 min in a freshly prepared solution of 75 mg/mL EDC and 21 mg/mL NHS in 500 μL dH_2O, then rinsed with dH_2O. NH_2-conjugated ssDNA probes (500 nM, TibMolBiol, SI Suppl. Table 1) were immobilized on the sensor surface for 1 h. Complementary ssDNA (TibMolBiol) was introduced via a peristaltic pump (40 μL/min) for 20 min at concentrations of 0.1, 1, 10, and 50 nM (See SI section 3). The sensor surface was washed with 0.01xPBS for 10 min after each step. The same strategy was used for patient samples (Fig. 2a). To evaluate the gFET device for the detection of SARS-CoV-2 RNA, 213 nasopharyngeal leftover samples with existing semiquantitative RT-PCR results from past routine testing were used. Specificity testing was performed on 21 pre-pandemic samples that tested positive for respiratory viruses other than SARS-CoV-2 (see SI section 1.1).

Following the functionalization of the sensor device with affinity binders for the target analyte, a sample volume of 400 μl was flowed over its surface for each test. FET transfer characteristics of the sensor device were recorded after a 20-min stabilization period (Fig. 2b, c and Suppl. Fig. 10). The binding event to the graphene channel was monitored from induced local electric field changes that are ascribed to surface charge density variations modulating the output current of the FET system. Transfer characteristics were obtained by sweeping the gate voltage (V_G) from −0.8V to 0.8V. To determine nucleic acid detection sensitivity, residual clinical patient samples were tested on the gFET biosensor setup functionalized with synthetic single-stranded DNA (ssDNA) complementary to the SARS-CoV-2 E-gene RNA (Corman et al., 2020). Higher voltages were not tested to avoid damaging biological components. For each step, time was kept constant at 20 min. Shifts corresponding to ΔV_{Dirac} (Fig. 2b and c) are caused by changes in the overall charge neutrality point due to doping effects from DNA/viral RNA hybridization (Szunerits et al., 2023).

The SARS-CoV-2 RT-PCR results and corresponding E-gene gFET read-outs were categorized by RT-PCR Ct values (Fig. 2d). Samples with Ct values of 12–19 ($n = 13$) showed mean gFET read-outs of 0.21 V with a standard deviation (SD) of 0.04 V. Samples with Ct values of 20–29 ($n = 10$) and of 30–39 ($n = 9$) had respective mean gFET read-outs of 0.18 V (SD ± 0.06 V) and 0.06 V (SD ± 0.03 V). For 160 SARS-CoV-2 RNA-negative samples tested in pools of 5, the mean gFET read-out was 0.03 V (SD ± 0.01 V). Even at higher Ct values, such as 38.9, the positive samples continued to elicit higher gFET responses (0.06) than the negative samples (0.04). Statistical analysis for assay sensitivity and specificity was performed by applying ROC curve analysis. Calculations for all samples, and excluding the RT-PCR positive samples with Ct values > 35 ($n = 7$), showed a sensitivity of 81.25% and 96.00% and specificity of 96.87% and 100.00% (AUC 0.908 and 0.974), respectively ($p < 0.001$; See SI section 7, Suppl. Fig. 14b). Linearity of RT-PCR positive samples against gFET readout ($n = 32$) was tested by rank correlation, revealing a Spearman's coefficient of rank correlation (rho) of −0.914 (95% confidence interval −0.958 to −0.830; $p < 0.0001$; Suppl. Fig. 14a). By testing samples containing respiratory viruses other than SARS-CoV-2 (see SI section1.1), the gFET assay demonstrated remarkable SARS-CoV-2 specificity, as indicated by the uniform read-outs of 0.02 V (±0.01 V) across the three pools, aligning with the voltage range established for SARS-CoV-2 negative samples (Fig. 2e). This consistency in results underscores the assay's ability to accurately discriminate the presence of SARS-CoV-2 amidst a background of other respiratory pathogens.

3.2. Biosensor measurements in context with virus culture, RT-PCR, patient medical history and sampling timepoints

Anti-SARS-CoV-2 nucleocapsid protein antibody (Abcam) was immobilized using EDC-NHS chemistry (Fig. 3a, Suppl. Fig. 6). A PyPEG/PyCOOH ratio (1:9) was used for functionalization. Affinity interaction with recombinantly expressed N-protein was tested (Fig. 3a; SI 3.2). From the measured transfer characteristics data (Fig. 3b), the calibration curve was established (Fig. 3c) and the respective limit of detection (LOD) was determined. The alteration in the current response ΔI on the anti-N Ab functionalized graphene surface was plotted against the analyte concentrations of 0.1 pM, 1 pM, 10 pM, 100 pM, 1 nM, 10 nM, and 100 nM in log scale and fitted by a linear function with a slope S = 6 μA/pM. The LOD was determined from the intersection of the fitted

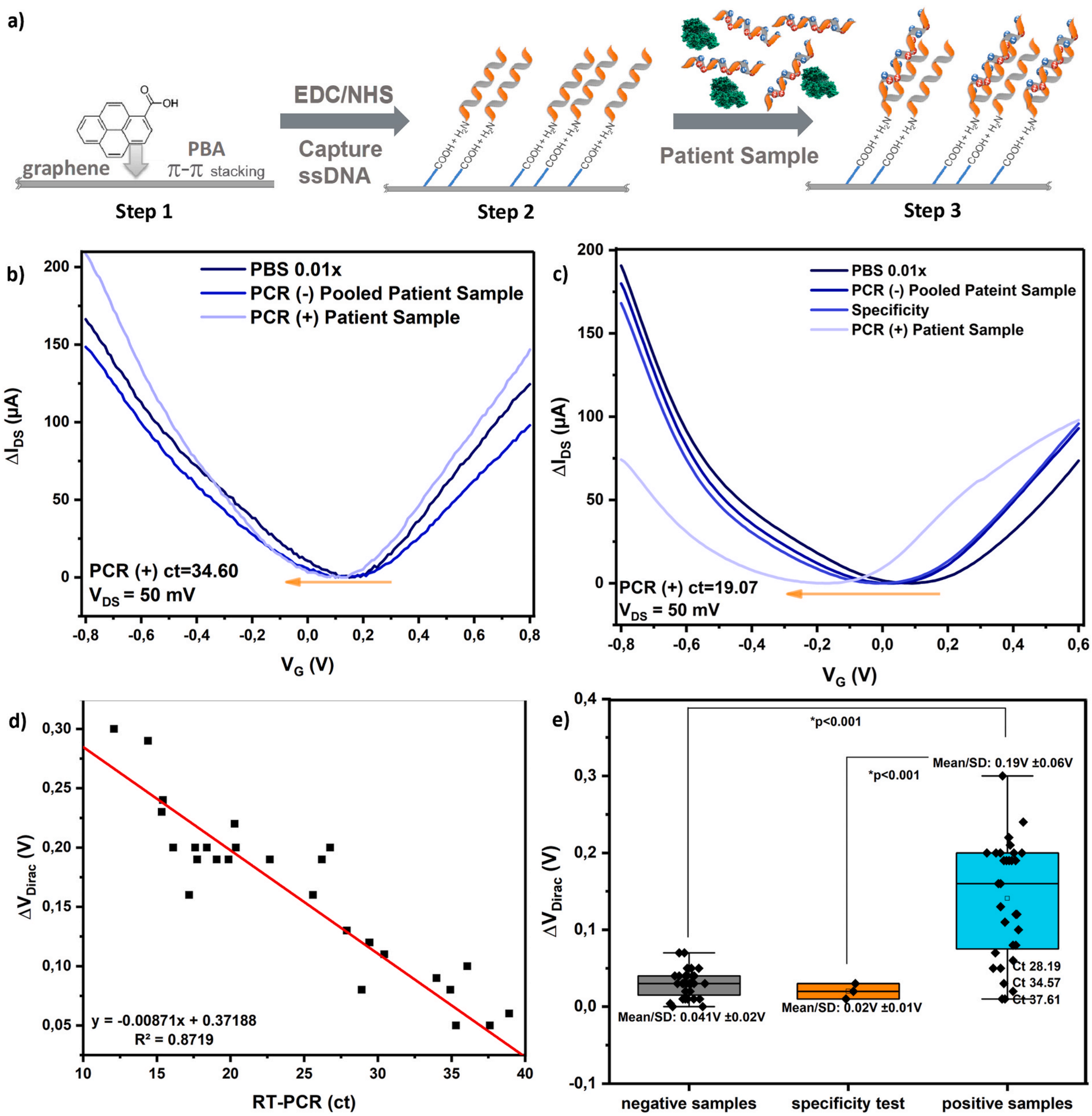

Fig. 2. Detailed analysis of a graphene-coated sensor designed for DNA/RNA hybridization in the detection of SARS-CoV-2. a) Schematic of the sensor functionalization process: starting with a bare rGO sensor, attaching phenolic hydroxyl groups (step 1), activation with EDC/NHS and anchoring specific bio-recognition elements for DNA/RNA hybridization (e.g. ssDNA; step 2), and exposing the sensor to a complex sample, leading to specific binding of target RNA to capture ssDNA (step 3). **b)** Averaged transfer characteristic curves for a SARS-CoV-2 positive patient sample (Ct 34.6) from 10 IdVg measurements, showing consistent sensor response and reduced signal drift. **c)** Averaged transfer characteristic curves for a SARS-CoV-2 positive patient sample (Ct 19.07) and specificity tests with pooled patient samples, demonstrating the sensor's sensitivity and specificity. **d)** Correlation between biosensor signal change (ΔVDirac) and RT-PCR Ct values, with a high R^2 value, indicating reliable detection of viral load. **e)** Box plot comparing biosensor responses to negative and positive samples, demonstrating clear segregation and validating the sensor's discriminative power with significant p-values ($p < 0.001$).

calibration curve with 3.3 times the standard deviation of the background divided by the slope of the curve; 3.3 x $\left(\frac{\sigma(I)}{S}\right)$, where σ(I) = 1,8272 μA. The achieved (average) LOD was 0.9 pM and the LOQ was 2.8 pM. For measurements in complex media (Fig. 3d), we tracked changes in source-drain current (I_{DS}) instead of Dirac point shifts, reflecting local variations in mobility and carrier density (Fig. 3e & f). This method demonstrated infectivity changes at different infection stages more reliably using the change in output current at a constant output voltage of −400 mV (Suppl. Fig. 13). Biosensor measurements of patient samples with negative readouts from virus culture resulted in a change of 4.45 ± 1.9 μA in the current. Therefore 7 μA was determined as the experimental cut-off value for a positive gFET N-protein result indicating infectivity—a threshold that, when applied, revealed that all gFET results align with the results from the virus culture (Table 1, Fig. 3h, Suppl. Fig. 13). Fig. 3g presents biosensor measurement data from patients 1–6 across consecutive sampling periods, and corresponding demographic and medical history data are presented in Table 1. Specifically, for patient 1, the measured current on day 3 was 23.29 μA (infectious in cell culture), which significantly decreased to 2.17 μA (non-infectious in cell culture) by day 13. For patient 3, we measured a high initial current response of 50.6 μA (infectious in cell culture) on day 2, decreasing to 6.11 μA by day 11 (non-infectious in cell culture). While our results align with those from the virus culture, these

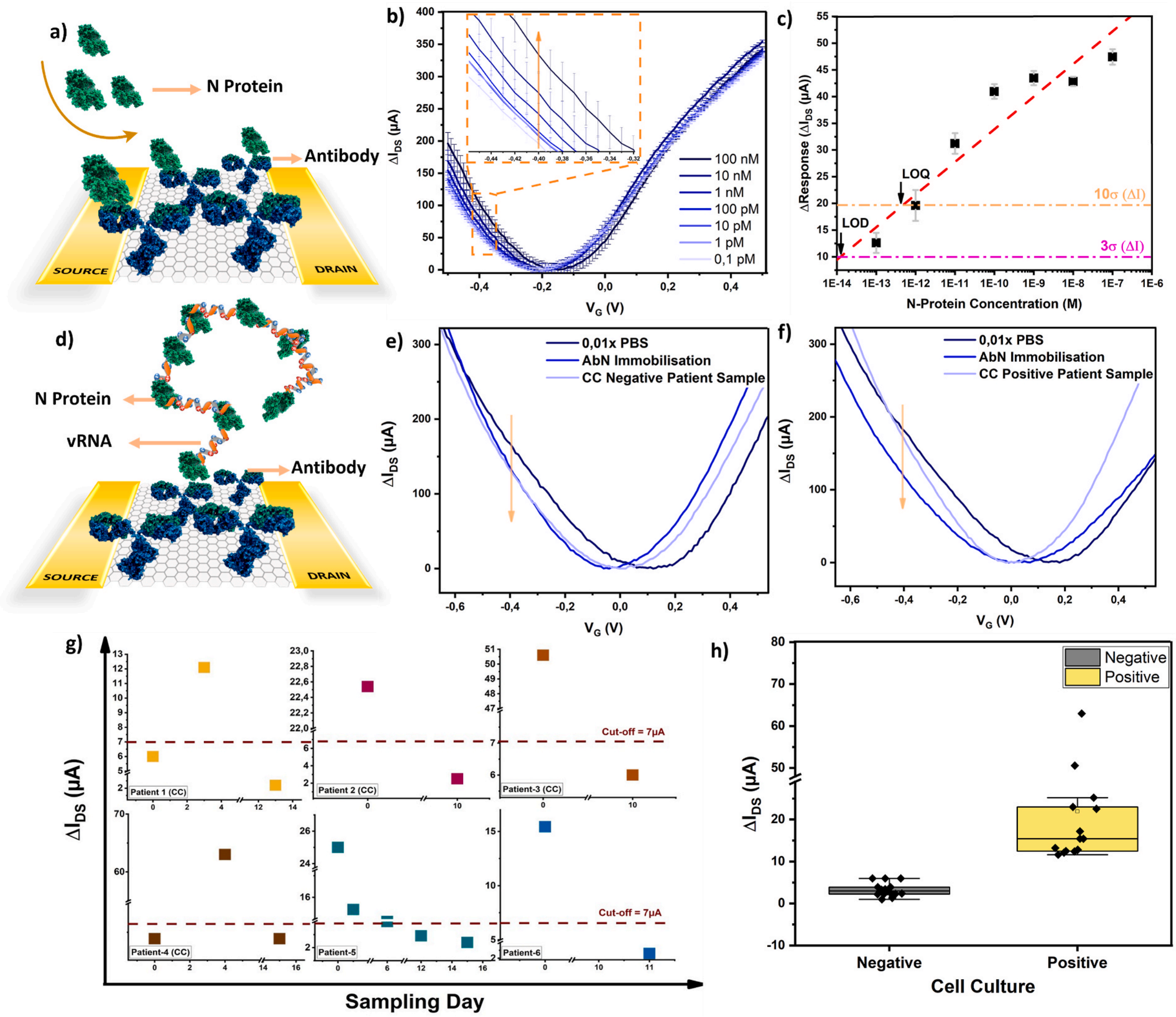

Fig. 3. Comprehensive Analysis of gFET Biosensor for Nucleocapsid Protein Detection a) Schematic of gFET biosensor with Anti-N Ab immobilized on graphene, showing the interaction with the N-protein. **b)** Transfer characteristic curves demonstrating the biosensor's electrical response to N-protein concentrations ranging from 0.1 pM to 100 nM. **c)** Calibration curve detailing the biosensor's response to incremental N-protein concentrations, indicating the limit of detection (LOD) and limit of quantification (LOQ). **d)** Illustration of N-protein binding to adjacent N-proteins via viral RNA. **e), f)** Transfer characteristic measurements for cell culture controls (negative and positive) and patient samples, showing the sensor's response to N-protein presence. **g)** Longitudinal study of 6 patients with samples taken over consecutive days, indicating biosensor response with a 7 μA cut-off for detection. h) Box plot comparing current changes in known positive and negative cell culture samples, illustrating the biosensor's diagnostic efficacy and ability to discriminate between positive and negative samples.

patients would have been categorized as infectious at both time points when applying the RT-PCR Ct 30 threshold. The opposite would be true for patient 5 and 16 who showed typical COVID-19 symptoms but Ct values > 30 on the day of admission. Declining Ct values in subsequent RT-PCR analysis reinforced the hypothesis that the patients were in the initial stages of their illness or within the incubation period, which was confirmed by the gFET result, indicating the presence of replicative virus. Patient 4 displayed conflicting results, as our initial measurement of 3.9 μA (non-infectious) on day 2 contrasted with clinical presentation and the onset of typical COVID-19 symptoms 2 days before RT-PCR testing, definitively indicating infectiousness. We consequently retested the sample with RT-PCR and noted a Ct shift of 3.7 in comparison to the initial result (initial Ct 29.9; repeated measurement 33.6). As our follow-up gFET results were consistent with the clinical course and the virus culture results, we concluded that this sample was likely damaged through storage conditions.

Three patients (patients 10, 17, 18; for patient history of 17 and 18 see SI section 6) with comorbidities were included, as discrimination of infectiousness is most difficult in immunocompromised and/or immunosuppressed patients with prolonged SARS-CoV-2 RNA detection. Patient 10, a multimorbid male presenting with a urinary tract infection, was diagnosed with SARS-CoV-2 infection 66 days before hospital admission. He showed intermittent low positive (nadir Ct 28.64 on day 2; mean Ct 35.56 SD ± 1.65) or negative RT-PCR results. Virus culture and gFET assay results were negative, indicating prolonged SARS-CoV-2 RNA shedding.

4. Discussion

Detecting SARS-CoV-2 and assessing infectivity requires not only measuring viral load but also determining the presence of replication-competent virus, which cannot be achieved through RNA detection alone. The integration of graphene-based field-effect transistor (gFET) biosensors in clinical diagnostics has been limited by persistent challenges that impede their transition from basic science laboratories into clinical settings. Among these challenges are device-to-device variability (Reiner-Rozman et al., 2021), batch heterogeneity (Widodo et al., 2018; Kotlowski et al., 2018), intricacies of bioreceptor anchoring (Kissmann et al., 2022; Rodrigues et al., 2021), and extending the Debye length in biosensors (Nakatsuka et al., 2018). Our research underscores the critical need for detailed characterization of gFET sensors, encompassing both active and control measurement systems, to ensure accurate calibration and validation of these sensors (See SI Figs. 3 and 7). This calibration, in conjunction with the statistical analysis of gFET ensembles, ensures that our results are robust and can withstand the rigors of clinical application. Additionally, the choice of different evaluation parameters ΔV_{Dirac} vs I_{DS} for SARS-CoV-2 RNA and N protein detection is rooted in the fundamental differences in the biophysical nature of these molecules (heat inactivation disrupts the viral structure, leaving RNA in smaller, more isolated pieces. Non-heat-inactivated samples retain the N protein-RNA complex, which is larger and more structured (Batéjat et al., 2021)). The N protein-RNA complex significantly alters the electrostatic environment by compressing the Electrical Double Layer (EDL), leading to an increase in capacitance C and stronger electrostatic interactions. As a result, the current change (ΔI_{DS}) is a more reliable measure for detecting this complex, as it captures the combined effects of capacitance changes, Schottky-barrier modulation, and carrier mobility (Heller et al., 2008; Bard et al., 2022). This nuanced approach to selecting evaluation parameters ensures that the sensor's response is tailored to the specific molecular characteristics and emphasizing the importance and the novelty of the dual target detection.

Despite these challenges, our study demonstrates that with careful calibration and characterization, gFET biosensors can effectively overcome these hurdles. This is evident in our initial results, where the gFET system successfully matched RT-PCR in SARS-CoV-2 E-gene RNA detection. Here, gFET biosensor readouts correlated with semi-quantitative RT-PCR results and displayed good sensitivity and specificity, particularly in samples with RT-PCR Ct values lower than 35 (sensitivity 96%; specificity 100%) (See SI section 7). Biosensors based on different transduction mechanisms have already proven their sensitivity for the detection of SARS-CoV-2 RNA. However, for the toehold RNA scaffolds biosensor, a simple color assay described by Chakravarthy et al. (2021), clinical patient samples underwent an RNA extraction and an amplification step before detection (35 min), while our assay uses native clinical patient samples. RNA extraction was also necessary for the plasmonic nanoparticle biosensor for N-gene RNA (testing time of 10 min) described by Moitra et al. (2020). Similar to the work of Kashefi-Kheyrabadi et al. (2022) and Peng et al. (2021), our study employs biosensing systems based on modifications in the Dirac voltage for the detection of SARS-CoV-2 RNA. Both studies demonstrated the capability of biosensors to effectively differentiate between positive and negative samples. Our system extends these findings by providing not only discrimination between sample statuses but also semi-quantitative data, showing a linear correlation between the sensor response and the Ct values derived from PCR within 20 min without prior steps.

The second aim of this study was to tackle infectivity diagnostics. The nucleocapsid (N-) protein is the most abundant protein in SARS-CoV-2 and packages viral RNA into structures necessary for replication and infectivity (Mencacci et al., 2021; Jack et al., 2021; Bai et al., 2021). It is a key antigen for detecting antibodies against SARS-CoV-2, enabling the identification of individuals who have previously been infected (Klausberger et al., 2021). Our study presents strong evidence to utilize the N-protein as a reliable marker for infectious viruses, as it aligns exceptionally well (100%) with virus culture results, thereby emphasizing its role in indicating potential infectivity. As corroborated by our gFET data, shedding of infectious virus can last over 20 days in virus culture, especially in immunosuppressed patients, and viral RNA has been detected months after first diagnosis of SARS-CoV-2 with Ct values sometimes below 20 (Aydillo et al., 2020; Raglow et al., 2024). While virus cultures are generally considered useful proxies for infectivity (Puhach et al., 2023; Jefferson et al., 2023), these techniques have important limitations, including a minimum viral load in the original sample (5.4 $\log_{10}$ genome copies/ml (Huang et al., 2020); Ct $\leq$ 32 (Raglow et al., 2024)). Respiratory swab samples tested at or near COVID-19 diagnosis are mostly, but not always, found to be positive via virus culture (Aydillo et al., 2020). This was consistent with our gFET data from samples early in infection. In contrast to virus culture, which remains the gold standard for infectivity determination, our gFET sensor is much faster, can be used in more frequently accessible BSL-2 laboratories, and requires no special media. Other biosensors for N-protein were reported with similar testing time (Aptamer functionalized gFET, 20min; Nanobody functionalized accumulation-mode OECT, 15min and sensitivity, but have been tested only in samples spiked with commercially available N-protein (Ban et al., 2022) or in very few patient samples (Guo et al., 2021), respectively.

Limiting factors of this study were the retrospective design including the uncertain consequences of sample storage conditions as well as the fact that virus propagation in culture required the use of special media and consequently separate swabs were needed. Another limitation was that our data did not allow separate analyses of SARS-CoV-2 variants, particularly given that Frediani et al. (2024) () highlighted that peak viral load time points differ between SARS-CoV-2 variants. Therefore, future studies should explore comparative analyses between different SARS-CoV-2 variants to decipher the dynamics of N-protein positivity. To the best of our knowledge, this is the first study to combine gFET biosensing data with the medical history of clinical patient samples and known time points during COVID-19 infection and implementing dual target detection. These results demonstrate that gFET biosensor detection shows comparable sensitivity to RT-PCR and provides additional information on the presence of viral antigens. This could benefit clinicians in discriminating whether a patient is shedding infectious virus or just residual viral RNA. Crucial clinical decisions, including whether a patient can receive immunotherapy or can be moved to a specialized unit like oncology or a care facility, need to be based on patient infectiousness. Long-term isolation can impact patient care and psychological health, as well as hospital resources. Our technology offers insights into the progression of viral infectivity, with potential applications in virological basic science and clinical diagnostics. Future prospective research should aim to validate the performance of biosensors against these clinical outcomes to further ensure their efficacy in real-world settings. Beyond that, the assay type can readily be adapted to rapidly detect other nucleic acids or proteins, for applications in any molecular biology field.

5. Conclusion

This study reports successful development of a gFET biosensor capable of dual target detection for SARS-CoV-2 markers with high sensitivity and specificity. The biosensor demonstrated dual detection capabilities: identifying SARS-CoV-2 RNA for diagnosing positivity and detecting nucleocapsid (N-) protein to assess patient infectiousness. The sensor's performance showed a strong correlation with RT-PCR cycle threshold (Ct) values (Spearman's rho $= -0.914$, $p < 0.0001$), and it exhibited a sensitivity of 96% and specificity of 100% for samples with Ct values below 35. Additionally, the gFET results were consistent with virus culture outcomes, particularly in distinguishing between infectious and non-infectious samples, further validated by an average limit of detection (LOD) of 0.9 pM for the N-protein. Importantly, the study overcame challenges related to batch-to-batch variability, ensuring consistent and reliable sensor performance across different production batches. While the biosensor has shown strong clinical utility, future work should validate its effectiveness across various SARS-CoV-2 variants and explore its application to other pathogens. Further research should also focus on integrating this technology into routine clinical diagnostics to enhance rapid decision-making in patient care.

6. Ethics

The study was conducted in accordance with the Declaration of Helsinki, after approval by the Ethics Committee of the Medical

University of Vienna (permit number: 1928/2020).

CRediT authorship contribution statement

Anna Nele Herdina: Writing – review & editing, Writing – original draft, Validation, Project administration, Methodology, Investigation, Funding acquisition, Formal analysis, Data curation, Conceptualization. **Anil Bozdogan:** Writing – review & editing, Writing – original draft, Visualization, Validation, Methodology, Investigation, Formal analysis, Data curation, Conceptualization, Project administration, Supervision. **Patrik Aspermair:** Writing – review & editing, Software, Project administration, Methodology, Funding acquisition, Conceptualization. **Jakub Dostalek:** Writing – review & editing, Validation, Supervision, Resources, Methodology, Investigation. **Miriam Klausberger:** Writing – review & editing, Supervision, Resources, Project administration, Methodology, Investigation, Funding acquisition, Formal analysis, Conceptualization. **Nico Lingg:** Writing – review & editing, Validation, Resources, Methodology, Formal analysis. **Monika Cserjan-Puschmann:** Writing – review & editing, Validation, Resources, Methodology, Formal analysis. **Patricia Pereira Aguilar:** Writing – review & editing, Validation, Resources, Methodology, Formal analysis. **Simone Auer:** Writing – review & editing, Methodology, Investigation, Formal analysis. **Halil Demirtas:** Writing – review & editing, Methodology, Formal analysis. **Jakob Andersson:** Writing – review & editing, Project administration, Methodology, Investigation, Funding acquisition, Conceptualization. **Felix Lötsch:** Writing – review & editing, Resources, Investigation, Formal analysis, Data curation. **Barbara Holzer:** Writing – review & editing, Validation, Resources, Methodology, Formal analysis. **Adi Steinrigl:** Writing – review & editing, Validation, Resources, Methodology, Formal analysis. **Florian Thalhammer:** Writing – review & editing, Validation, Resources, Methodology, Investigation. **Julia Schellnegger:** Writing – review & editing, Methodology, Formal analysis, Data curation. **Monika Breuer:** Writing – review & editing, Methodology, Formal analysis, Data curation. **Wolfgang Knoll:** Writing – review & editing, Supervision, Methodology, Investigation. **Robert Strassl:** Writing – review & editing, Writing – original draft, Supervision, Resources, Project administration, Methodology, Investigation, Funding acquisition, Formal analysis, Conceptualization.

Declaration of competing interest

The authors declare the following financial interests/personal relationships which may be considered as potential competing interests: Dr. Robert Strassl reports financial support was provided by Austrian Science Fund. If there are other authors, they declare that they have no known competing financial interests or personal relationships that could have appeared to influence the work reported in this paper.

Data availability

Data will be made available on request, except confidential patient data

Acknowledgements

This research was funded in whole by the Austrian Science Fund (FWF) [P 35103-B, Grant-DOI: 10.55776/P35103]. For open access purposes, the author has applied a CC BY public copyright license to any author-accepted manuscript version arising from this submission. We would like to thank Olfert Landt for advice on ssDNA probe design; Rui Qiang Chen, Jennifer Stock, and Christine Wukotitsch for their excellent support with ONT sequencing; Christoph Köppl and Andreas Fischer for excellent support in recombinant N protein expression and purification; and the whole team at the division of clinical virology for their support with standard diagnostics.

Appendix A. Supplementary data

Supplementary data to this article can be found online at https://doi.org/10.1016/j.bios.2024.116807.

References

Arnaout, R., Lee, R.A., Lee, G.R., et al., 2021. Clin. Infect. Dis. 73, e3042–e3046. https://doi.org/10.1093/cid/ciaa1382.

Avanzato, V.A., Matson, M.J., Seifert, S.N., et al., 2020. Cell 183, 1901–1912. e9. https://doi.org/10.1016/j.cell.2020.10.049.

Aydillo, T., Gonzalez-Reiche, A.S., Aslam, S., et al., 2020. N. Engl. J. Med. 383, 2586–2588. https://doi.org/10.1056/NEJMc2031670.

Bai, Z., Cao, Y., Liu, W., et al., 2021. Viruses 13. https://doi.org/10.3390/v13061115.

Ban, D.K., Bodily, T., Karkisaval, A.G., et al., 2022. Proceedings of the, vol. 119. National Academy of Sciences, e2206521119. https://doi.org/10.1073/pnas.220652111.

Bard, A.J., Faulkner, L.R., White, H.S., 2022. John Wiley & Sons. ISBN 0-471-04372-9.

Batéjat, C., Grassin, Q., Manuguerra, J.-C., et al., 2021. Journal of Biosafety and Biosecurity, vol. 3, pp. 1–3. https://doi.org/10.1016/j.jobb.2020.12.001.

Chakravarthy, A., Nandakumar, A., George, G., et al., 2021. Life Sci. Alliance 4. https://doi.org/10.26508/lsa.202101213.

Compans, R.W., Choppin, P.W., 1967. Proc Natl Acad Sci U S A 57 (4), 949–956. https://doi.org/10.1073/pnas.57.4.949.

Corman, V.M., Landt, O., Kaiser, M., et al., 2020. Euro Surveill. 25, 2000045. https://doi.org/10.2807/1560-7917.ES.2020.25.3.2000045.

Diao, B., Wen, K., Zhang, J., et al., 2021. Clin. Microbiol. Infection 27, 289. e1–e289. e4. https://doi.org/10.1016/j.cmi.2020.09.057.

Djaileb, A, Charron, B, Jodaylami, MH, Thibault, V, Coutu, J, Stevenson, K, et al., 2020. ChemRxiv. https://doi.org/10.26434/chemrxiv.12118914.v1.

Frediani, J.K., Parsons, R., McLendon, K.B., et al., 2024. Clin. Infect. Dis. 78, 301–307. https://doi.org/10.1101/2023.05.09.23289735.

Gaspar, L.P., Terezan, A.F., Pinheiro, A.S., et al., 2001. J. Biol. Chem. 276 (10), 7415–7421. https://doi.org/10.1074/jbc.M010037200, 9.

Guo, K., Wustoni, S., Koklu, A., et al., 2021. Nat. Biomed. Eng. 5, 666–677. https://doi.org/10.1038/s41551-021-00734-9.

Hasler, R., 2022. ACS Sens. 7, 504–512. https://doi.org/10.1021/acssensors.1c02313.

Heller, I., Janssens, A.M., Männik, J., et al., 2008. Nano Lett. 8, 591–595. https://doi.org/10.1021/nl072996i.

Huang, C.-G., Lee, K.-M., Hsiao, M.-J., et al., 2020. J. Clin. Microbiol. 58. https://doi.org/10.1128/jcm.01068-20.

Jack, A., Ferro, L.S., Trnka, M.J., et al., 2021. PLoS Biol. 19, e3001425. https://doi.org/10.1371/journal.pbio.3001425.

Jefferson, T., Spencer, E.A., Conly, J.M., Rosca, E.C., Maltoni, S., Brassey, J., Plüddemann, A., 2023. J. Hosp. Infect. 132, 62–72. https://doi.org/10.1016/j.jhin.2022.11.018.

Karkan, S.F., Baladi, R.M., Shahgolzari, M., et al., 2022. J. Virol Methods 300, 114381. https://doi.org/10.1016/j.jviromet.2021.114381.

Kashefi-Kheyrabadi, L., Nguyen, H.V., Go, A., et al., 2022. Biosens. Bioelectron. 195, 113649. https://doi.org/10.1016/j.bios.2021.113649.

Kirby, J.E., Riedel, S., Dutta, S., et al., 2023. Clin. Microbiol. Infection 29, 94–100. https://doi.org/10.1016/j.cmi.2022.07.010.

Kissmann, A.-K., Andersson, J., Bozdogan, A., et al., 2022. Nanoscale Horizons 7, 770–778. https://doi.org/10.1039/D1NH00605C.

Klausberger, M., Duerkop, M., Haslacher, H., et al., 2021. EBioMedicine 67. https://doi.org/10.1016/j.ebiom.2021.103348.

Kotlowski, C., Aspermair, P., Khan, H.U., et al., 2018. Flex Print Electron, vol. 3, 034003. https://doi.org/10.1088/2058-8585/aad433.

Loveday, E.K., Hain, K.S., Kochetkova, I., et al., 2021. Viruses 13. https://doi.org/10.3390/v13040562.

Lu, S., Ye, Q., Singh, D., et al., 2020. bioRxiv. https://doi.org/10.1101/2020.07.30.228023.

Mahari, S., 2020. Cold Spring Harbor Laboratory. https://doi.org/10.1101/2020.04.24.059204.

Mathuria, JP, Yadav, R, 2020 Jul. J. Infect. Publ. Health 13 (7), 901–905. https://doi.org/10.1016/j.jiph.2020.06.005.

Mencacci, A., Gili, A., Gidari, A., et al., 2021. J. Clin. Med. 10, 4037. https://doi.org/10.3390/jcm10184037.

Moitra, P., Alafeef, M., Dighe, K., et al., 2020. ACS Nano 14, 7617–7627. https://doi.org/10.1021/acsnano.0c03822.

Muradyan, N., Arakelov, V., Sargsyan, A., et al., 2024. Sci. Rep. 14, 5870. https://doi.org/10.1038/s41598-024-55157-8.

Murugan, D., Bhatia, H., Sai, V.V.R., et al., P-FAB, 2020. Trans Indian Natl. Acad. Eng. 5, 211–215. https://doi.org/10.1007/s41403-020-00122-w.

Nakatsuka, N., Yang, K.-A., Abendroth, J.M., et al., 2018. Science 362, 319–324. https://doi.org/10.1126/science.aao6750.

Peng, Y., Pan, Y., Sun, Z., et al., 2021. Biosens. Bioelectron. 186, 113309. https://doi.org/10.1016/j.bios.2021.113309.

Puhach, O., Meyer, B., Eckerle, I., 2023. Nat. Rev. Microbiol. 21, 147–161. https://doi.org/10.1038/s41579-022-00822-w.

Qiu, G., 2020. ACS Nano. https://doi.org/10.1021/acsnano.0c02439.

Rabiee, N., 2020. Int. J. Mol. Sci. 21 (14), 5126. https://doi.org/10.3390/ijms21145126.

Raglow, Z., Surie, D., Chappell, J.D., et al., 2024. The Lancet Microbe. https://doi.org/10.1016/S2666-5247(23)00336-1.

Rampazzi, S., 2016. IEEE Trans. Instrum. Meas. 65, 317–327. https://doi.org/10.1109/TIM.2015.2465691.
Reiner-Rozman, C., Hasler, R., Andersson, J., et al., 2021. Micro & Nano Lett. 16, 436–442. https://doi.org/10.1049/mna2.12070.
Zhen, W., Smith, E., Manji, R., Schron, D., Berry, G.J., 2020. J. Clin. Microbiol. 58 (8), 10–1128. https://doi.org/10.1128/jcm.00783-20.
Rodrigues T, Mishyn V, Bozdogan A, et al. 2021; DOI: 10.47829/ACMCR.2021.6204.
Roether, J., 2019. Biosens. Bioelectron. 142. https://doi.org/10.1016/j.bios.2019.111528.
Seo, G., 2020. ACS Nano 14, 5135–5142. https://doi.org/10.1021/acsnano.0c02823.
Soler, M., 2020. ACS Sens. 5, 2663–2678. https://doi.org/10.1021/acssensors.0c01180.
Szunerits, S., Rodrigues, T., Bagale, R., et al., 2023. Anal. Bioanal. Chem. https://doi.org/10.1007/s00216-023-04760-1.
Widodo, C.S., Sela, H., Santosa, D.R., 2018. AIP Conf. Proc. 2021, 050003. https://doi.org/10.1063/1.5062753.
World Health Organisation WHO, 2021. Recommendations for National SARS-CoV-2 Testing Strategies and Diagnostic Capacities. Interim Guidance.
Wu, W., Cheng, Y., Zhou, H., et al., 2023. Virol. J. 20, 6. https://doi.org/10.1186/s12985-023-01968-6.